Supporting information for

Hindered Cluster Rotation and ^{45}Sc Hyperfine Splitting Constant in Distonoid Anion-Radical $Sc_3N@C_{80}^-$, and Spatial Spin-Charge Separation as a General Principle for Anions of Endohedral Fullerenes with Metal-Localized Lowest Unoccupied Molecular Orbital

Alexey A. Popov,[†] and Lothar Dunsch[‡]*

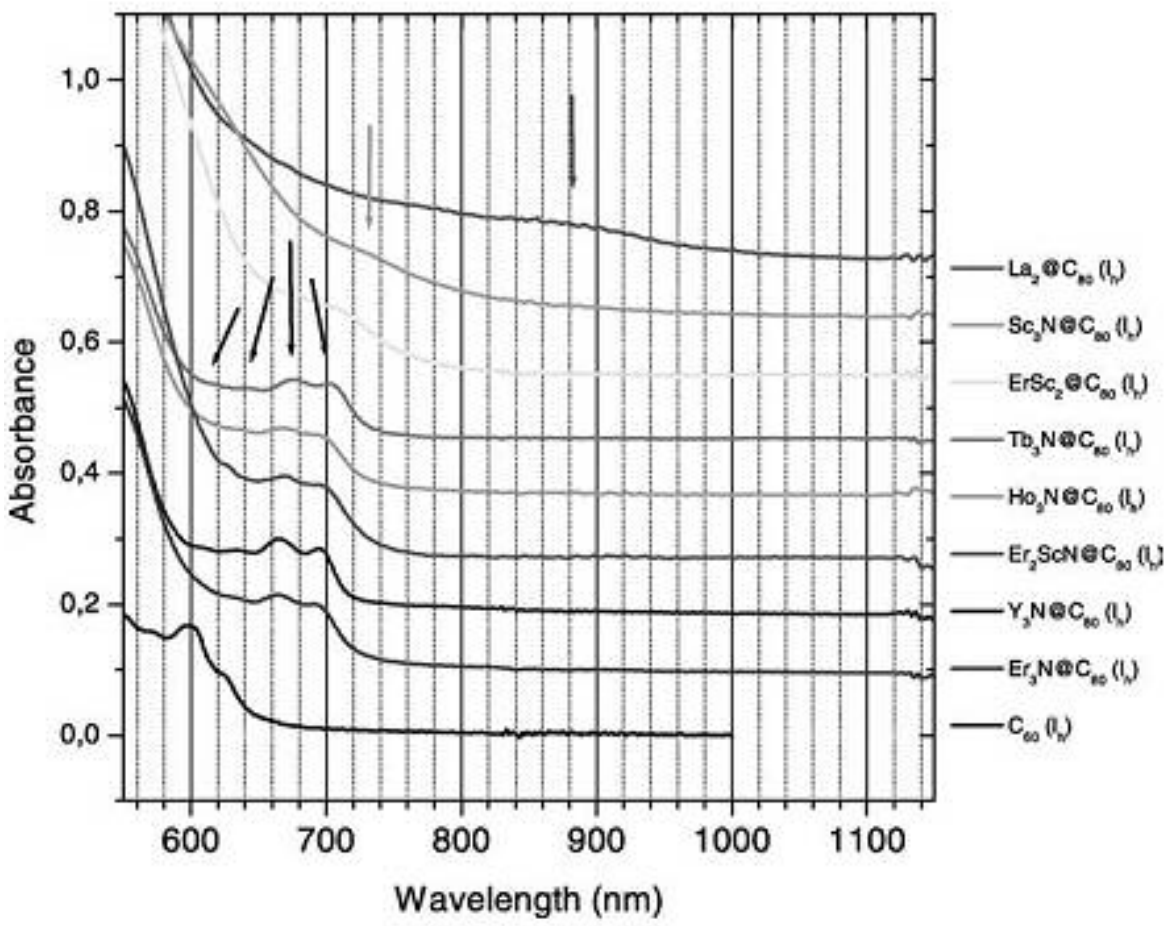

Figure S1 Absorption spectra of $Sc_3N@C_{80}$ and other $M_3N@C_{80}$ (from L. Dunsch et al, *J. Phys. Chem. Sol.* **2004**, *65*, 309)

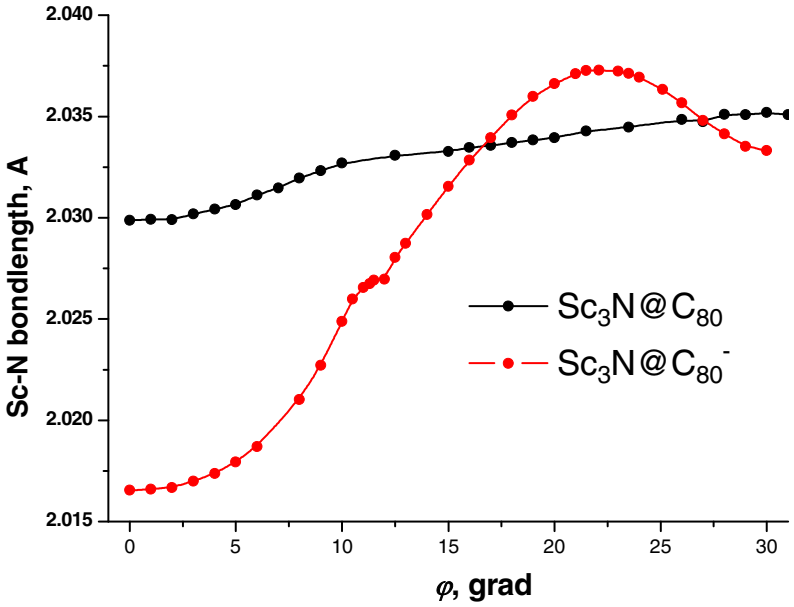

Figure S2. Changes of Sc–N bondlengths and pyramidalization of the cluster as a function of the cluster rotation angle φ in the neutral and charged states of $Sc_3N@C_{80}$.

Table S1. B3LYP//PBE-computed a(Sc) hfc and ΔE for $Sc_3N@C_{80}^-$ conformers as a function of the cluster rotation angle φ.

φ	a(Sc), G	ΔE, kJ/mol
0	28.53	0.0
5	27.74	7.8
10	30.46	28.1
11.3	34.99	31.9
13	25.27	30.8
15	14.03	28.6
17	5.29	26.8
20	-3.67	25.2
22.1	-7.48	23.7
25	-9.35	24.3
30	-6.18	26.0

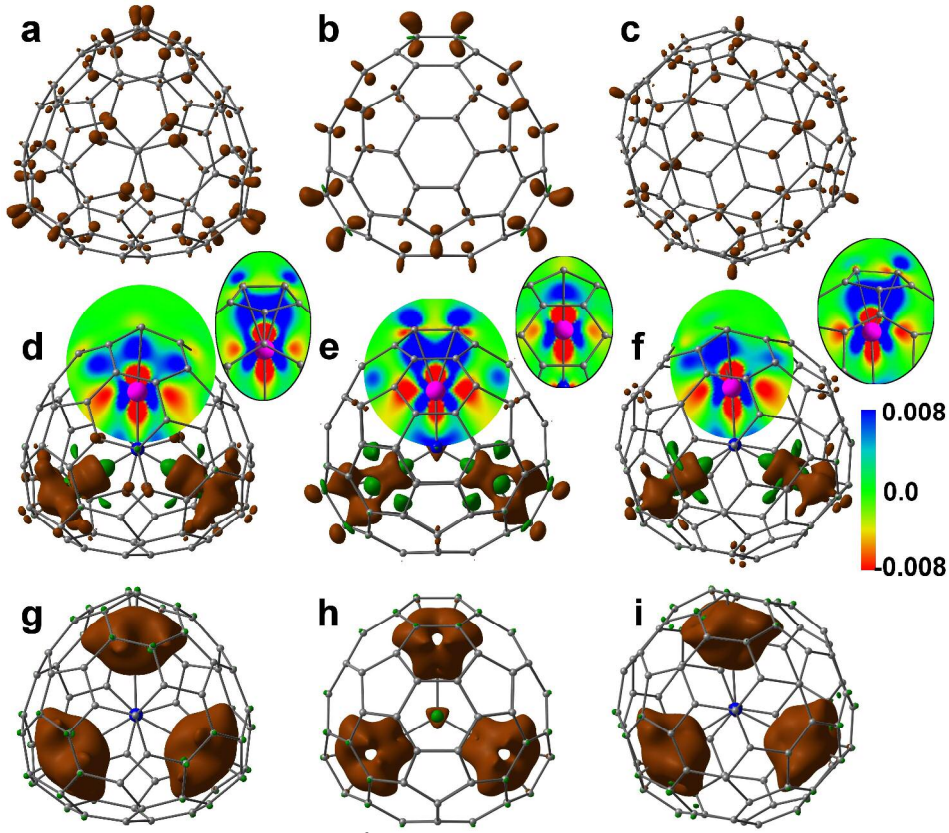

Figure S3. (a)-(c): $\rho(C_{2n}^{6-}) - \rho(C_{2n})$ for 2n=68 (a), 2n=78 (b), and 2n=80 (c);
(d)-(f): $\rho(Sc_3N@C_{2n}) - \rho(C_{2n}) - \rho(Sc_3N)$ for 2n=68 (d), 2n=78 (e), 2n=80 (f) (brown - positive, green - negative sign of difference density). Coordinates of C_{2n} and Sc_3N are constrained to their coordinates in $Sc_3N@C_{2n}$; for one of the Sc atoms in each molecule the difference density mapped on the cluster plane is shown, the insets also show difference density mapped on the perpendicular plane.
(g)-(i): $\rho(Sc_3N@C_{2n}) - \rho(C_{2n}^{6-}) - \rho(Sc_3N^{6+})$ for 2n=68 (g), 2n=78 (h), 2n=80 (i).

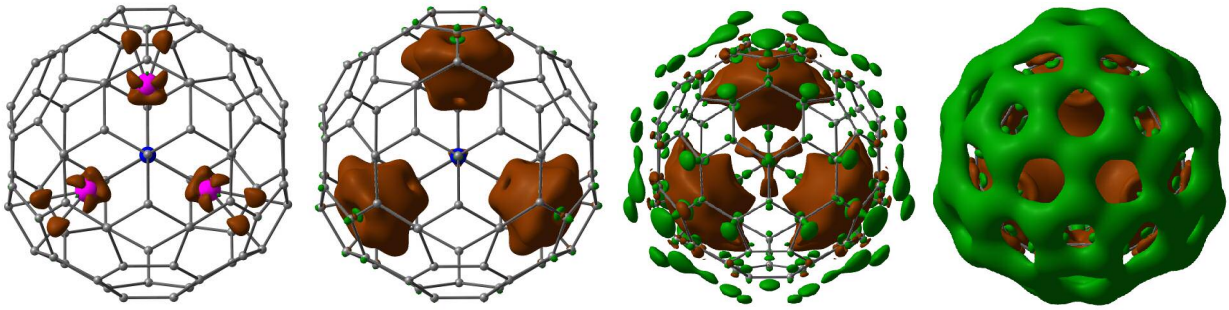

Figure S4. [$\rho(Sc_3N@C_{80}) - \rho(C_{80}^{6-}) - \rho(Sc_3N^{6+})$]) plotted with different values of isodensity.

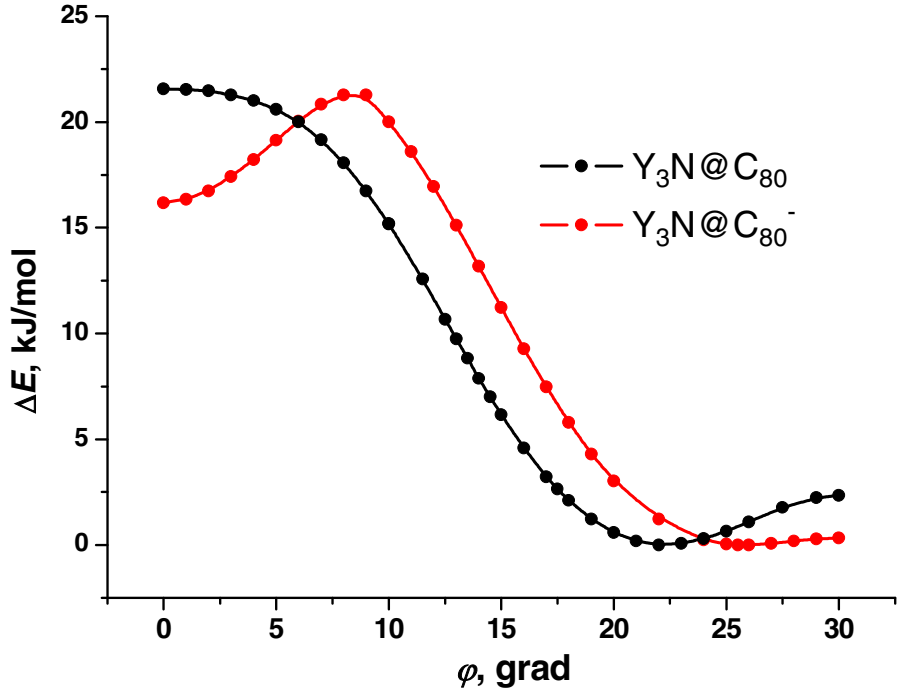

Figure S5. PBE/TZ2P-computed ΔE for the conformers of $Y_3N@C_{80}$ and $Y_3N@C_{80}^-$ as a function of the cluster rotation angle φ.

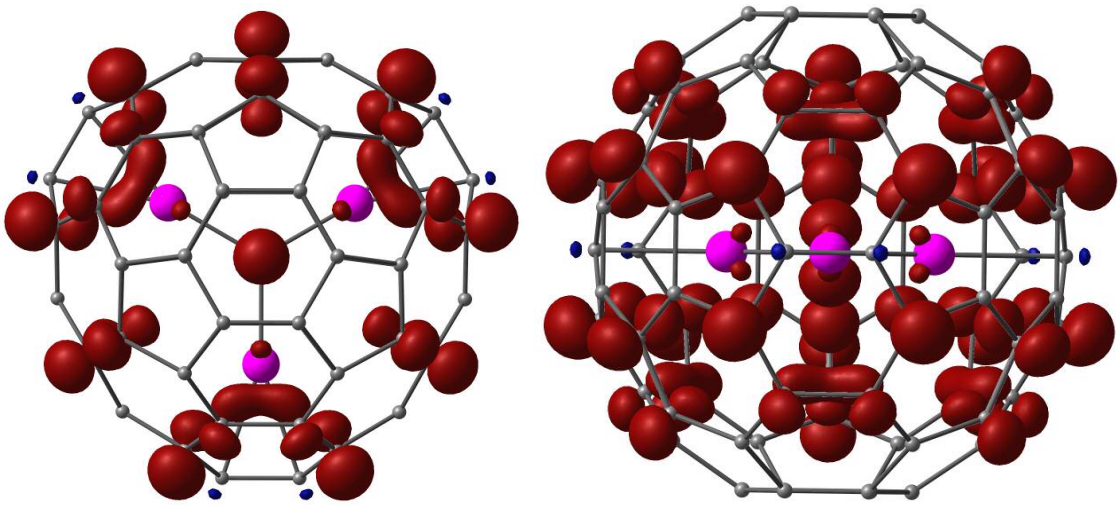

Figure S6a. Spin density in $Sc_3N@C_{78}^-$; Sc spin population −0.003, a(^{45}Sc)= −2.22 Gauss

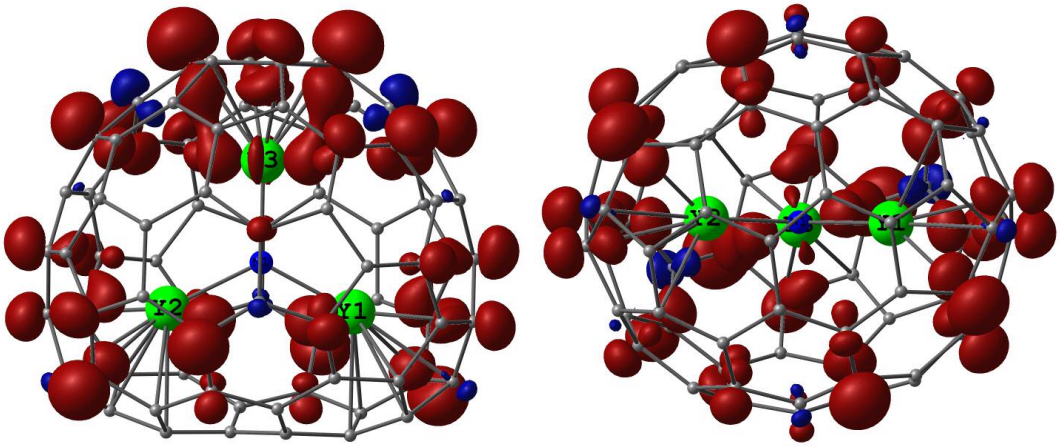

Figure S6b. Spin density in $Y_3N@C_{78}^-$, Y spin population: 0.01 on Y1 and Y2, 0.08 on Y3; a(^{89}Y)= −0.95 G for Y1 and Y2, −1.52 G for Y3

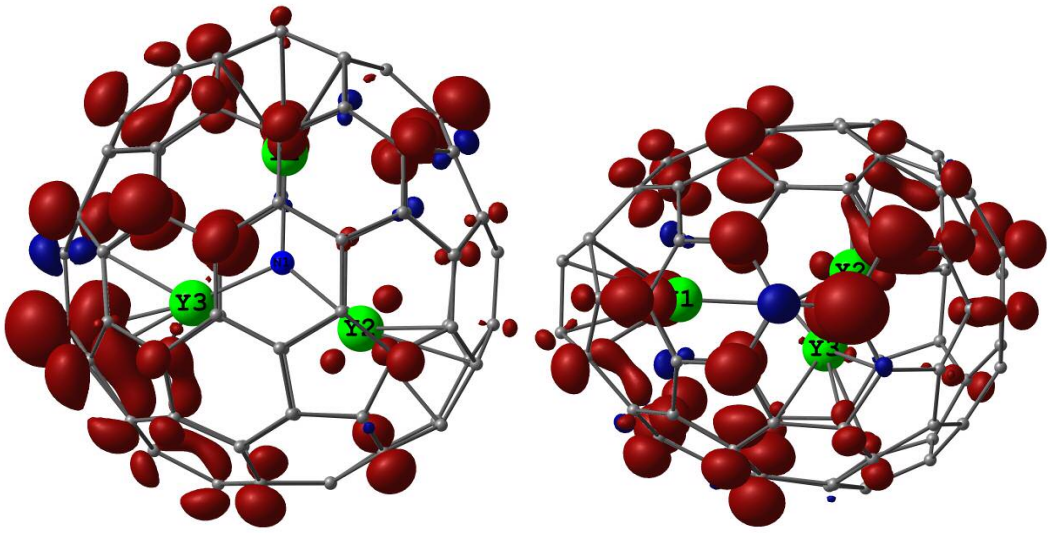

Figure S6c. Spin density in $Y_3N@C_{84}^-$; Y spin population: 0.01, 0.05, and 0.02 on Y1, Y2, and Y3, respectively; a(^{89}Y) = 0.72, −1.78, and −2.59 Gauss for Y1, Y2, and Y3, respectively.

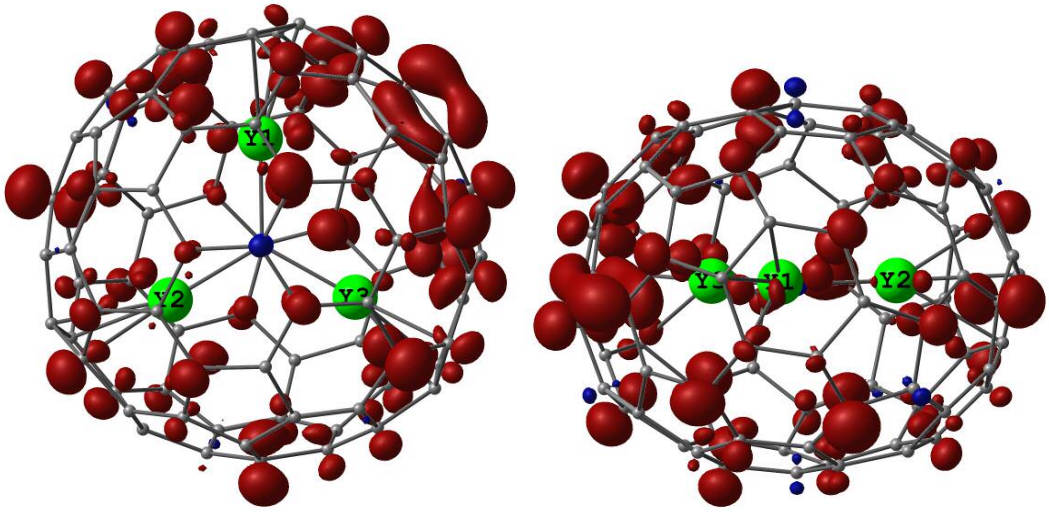

Figure S6d. Spin density in $Y_3N@C_{86}^-$; Y spin population: 0.04, 0.03, and 0.03 on Y1, Y2, and Y3, respectively; $a(^{89}Y)$ = –0.50, 0.04, and 0.88 Gauss for Y1, Y2, and Y3, respectively.

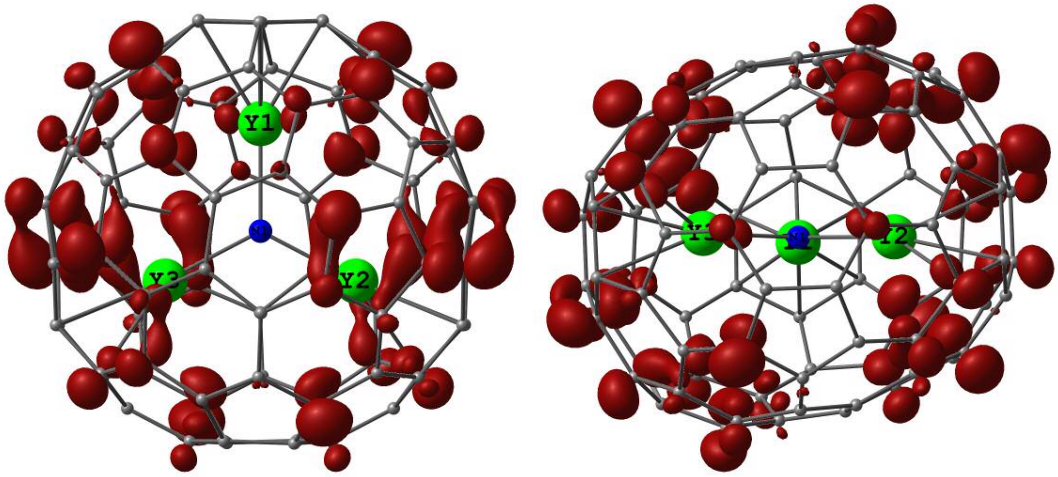

Figure S6e. Spin density in $Y_3N@C_{88}^-$. Spin population: 0.003 on Y1, 0.01 on Y2 and Y3; $a(^{89}Y)$=0.31 G for Y1 and 0.65 G for Y2 and Y3.

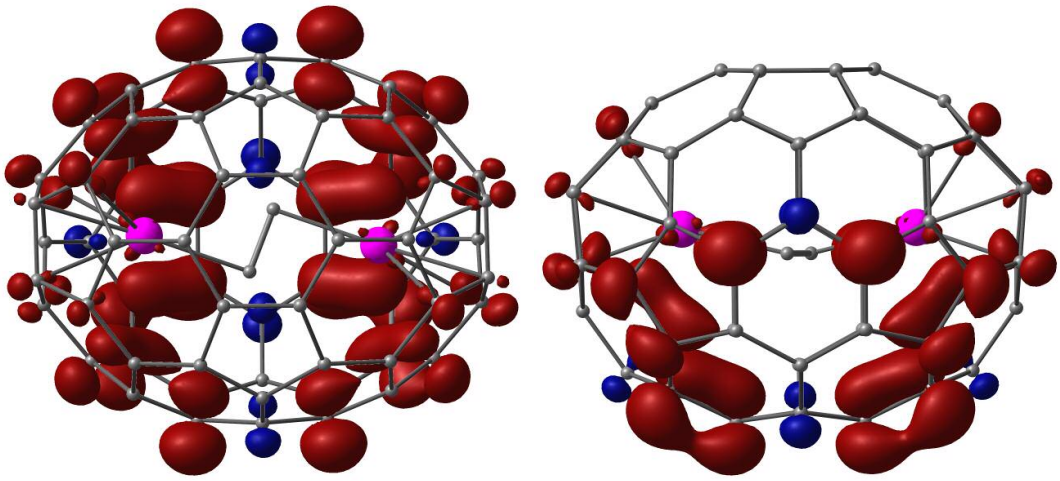

Figure S6f. Spin density in $Sc_2C_2@C_{68}^-$: Sc spin population 0.01; $a(^{45}Sc)$= –0.77 Gauss

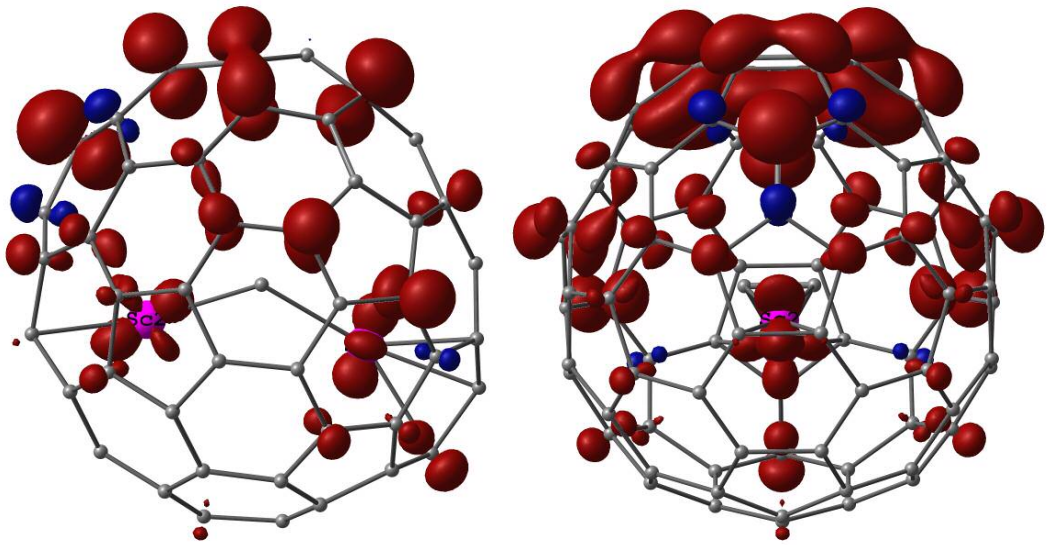

Figure S6g. Spin density in $Sc_2C_2@C_{82}^-$: Sc spin population 0.06 on Sc1 and 0.05 on Sc2; $a(^{45}Sc)$ = 8.62 for Sc1, and −1.13 G for Sc2.

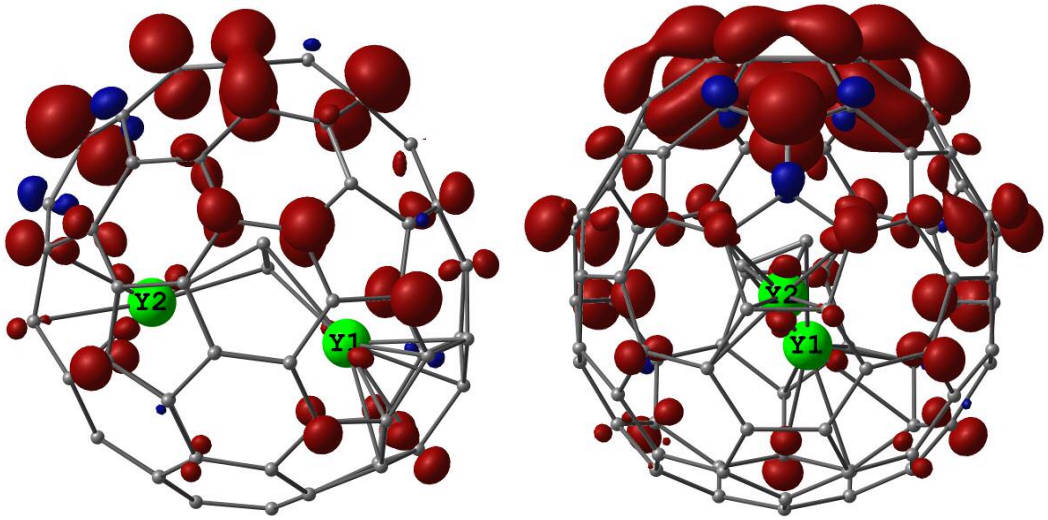

Figure S6h. Spin density in $Y_2C_2@C_{82}^-$; Y spin population: 0.03 on Y1 and 0.04 on Y2; $a(^{89}Y)$= 0.00 for Y1 and −0.74 G for Y2

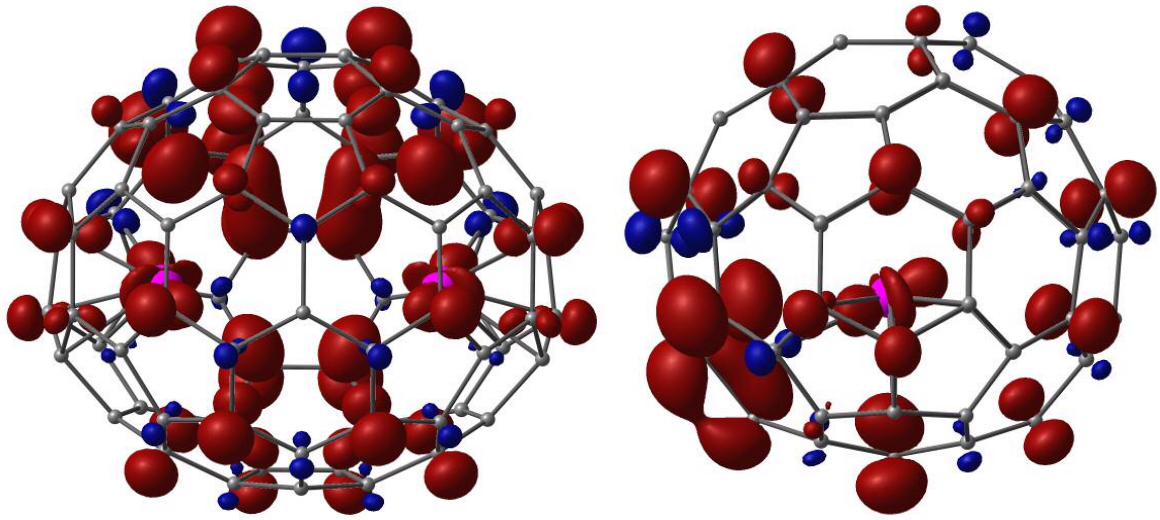

Figure S6i. Spin density in $Sc_2@C_{76}^-$. Sc spin population 0.05; $a(^{45}Sc)$ = −1.16 Gauss

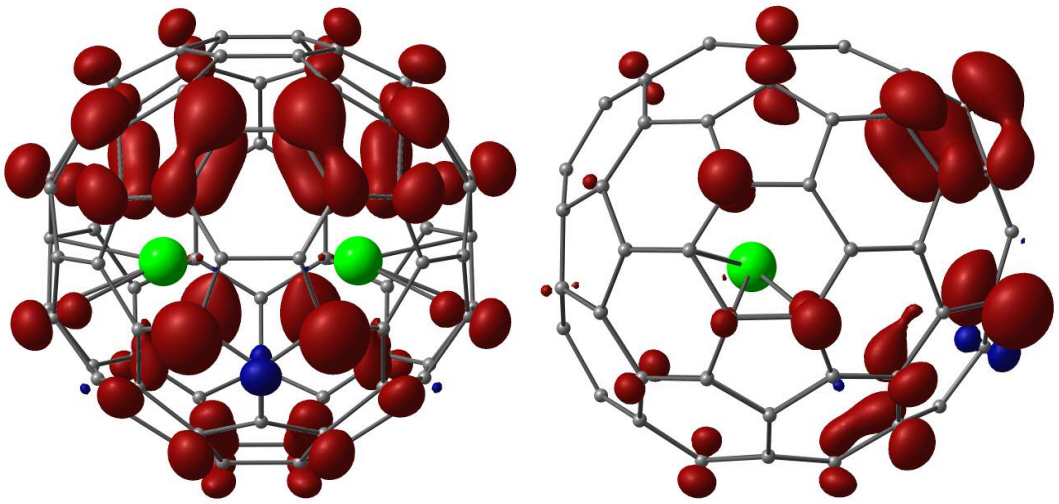

Figure S6j. Spin density in $Y_2@C_{82}^-$; Y spin population 0.01; $a(^{89}Y)$=1.63 Gauss

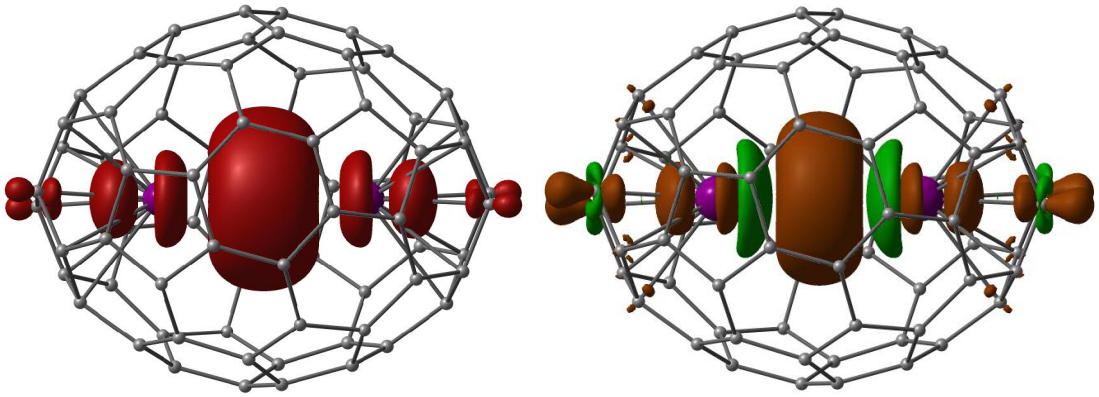

Figure S7a. Spin density in $La@C_{72}^-$ (left) and $\rho(La@C_{72}^-)-\rho(La@C_{72})$ (right)

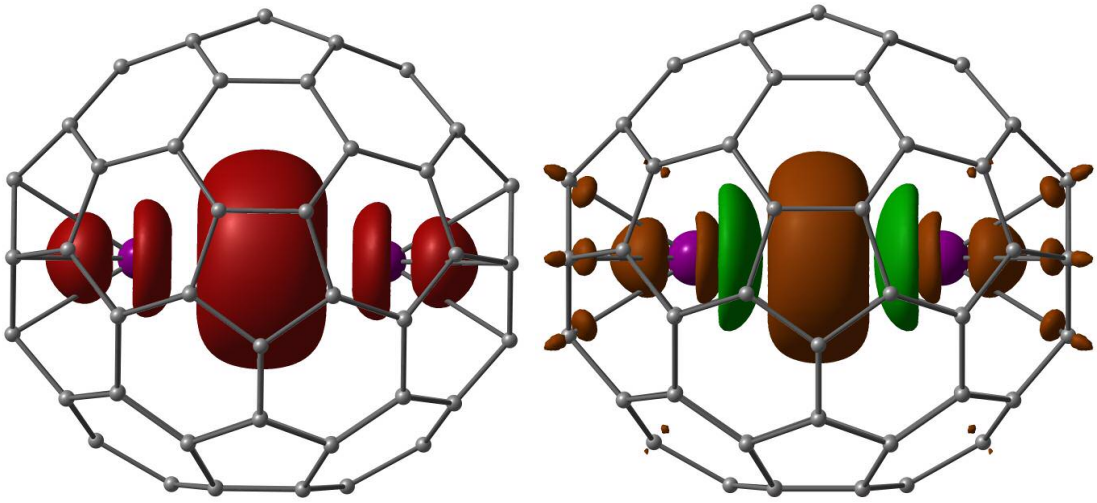

Figure S7b. Spin density in $La@C_{78}^-$ (left) and $\rho(La@C_{78}^-)-\rho(La@C_{78})$ (right)